APL Materials

Growth of $PdCoO_2$ by ozone-assisted molecular-beam epitaxy

Cite as: APL Mater. **7**, 121112 (2019); https://doi.org/10.1063/1.5130627
Submitted: 05 October 2019 • Accepted: 08 December 2019 • Published Online: 27 December 2019

Jiaxin Sun, Matthew R. Barone, Celesta S. Chang, et al.

Growth of $PdCoO_2$ by ozone-assisted molecular-beam epitaxy

Cite as: APL Mater. 7, 121112 (2019); doi: 10.1063/1.5130627
Submitted: 5 October 2019 • Accepted: 8 December 2019 •
Published Online: 27 December 2019

Jiaxin Sun,[1] Matthew R. Barone,[1] Celesta S. Chang,[2] Megan E. Holtz,[1] Hanjong Paik,[1,3] Jürgen Schubert,[4] David A. Muller,[5,6] and Darrell G. Schlom[1,6]

AFFILIATIONS

[1]Department of Materials Sciences and Engineering, Cornell University, Ithaca, New York 14853, USA
[2]Department of Physics, Cornell University, Ithaca, New York 14853, USA
[3]Platform for the Accelerated Realization, Analysis, and Discovery of Interface Materials (PARADIM), Cornell University, Ithaca, New York 14853, USA
[4]Peter Grünberg Institute (PGI-9) and JARA-Fundamentals of Future Information Technology, Forschungszentrum Jülich GmbH, 52425 Jülich, Germany
[5]School of Applied and Engineering Physics, Cornell University, Ithaca, New York 14853, USA
[6]Kavli Institute at Cornell for Nanoscale Science, Ithaca, New York 14853, USA

ABSTRACT

We report the *in situ*, direct epitaxial synthesis of (0001)-oriented $PdCoO_2$ thin films on *c*-plane sapphire using ozone-assisted molecular-beam epitaxy. The resulting films have smoothness, structural perfection, and electrical characteristics that rival the best *in situ* grown $PdCoO_2$ thin films in the literature. Metallic conductivity is observed in $PdCoO_2$ films as thin as ~2.0 nm. The $PdCoO_2$ films contain 180° in-plane rotation twins. Scanning transmission electron microscopy reveals that the growth of $PdCoO_2$ on the (0001) surface of Al_2O_3 begins with the CoO_2 layer.

The delafossite $PdCoO_2$ is distinguished by having the lowest in-plane resistivity ($\rho_{ab\,(4\,K)}$ = 7.5 nΩ cm) and longest mean free path ($\ell_{(4\,K)}$ = 21.4 μm) of all known oxide materials;[1] its conductivity at room temperature is even higher than elemental copper per carrier.[1] Moreover, this family of compounds hosts large spin-orbit coupling (SOC). A spin splitting of 60 meV and 120 meV of surface-derived bands arising from Rashba-like splitting has been observed on $PdCoO_2$ and $PdRhO_2$, respectively, using angle-resolved photoemission spectroscopy (ARPES).[2] The combination of a layered structure, long mean free path, low density of states (for a metal), and large SOC makes $PdCoO_2$ a promising candidate for the next generation of spintronic devices, such as in the proposed Magneto-Electric Spin-Orbit (MESO) logic architecture.[3]

The physics of $PdCoO_2$ and related metallic delafossites has been primarily studied using flux-grown single crystals that, despite decades of research, are still limited in size (~3 mm in diameter).[4–6] To facilitate further studies of its physical properties, particularly as its thickness is decreased down to a single formula unit, and the assessment of proof-of-principle spintronic devices, single crystals with large area and smooth surfaces in the form of thin films are needed. So far, $PdCoO_2$ has been synthesized in thin film form using sputtering,[7] pulsed-laser deposition (PLD),[8,9] and molecular-beam epitaxy (MBE).[10] Already the advantages of the thin-film growth have been demonstrated by the realization of a high-performance electronics device[11] and the observation of surface ferromagnetism at the ultrathin limit[12] based on $PdCoO_2$ films grown by PLD.[8]

A major challenge to the growth of $PdCoO_2$ is oxidizing the palladium. If we look to synthesis routes that have achieved high-quality $PdCoO_2$, the original method took place under 3000 atm of oxygen at 800 °C for 12 h.[13] Such conditions are clearly far from being compatible with vacuum deposition methods used to produce thin films, but subsequently a lower-pressure route was found that yields $PdCoO_2$ single crystals up to 3 mm in size involving the

reaction $PdCl_2 + 2\ CoO \rightarrow PdCoO_2 + CoCl_2$ in a sealed quartz tube at 700 °C for 40 h.[5,6]

Compared to the growth of bulk $PdCoO_2$, the pressures at which $PdCoO_2$ thin films have been made are much lower. Early sputtered films were deposited at pressures of 2×10^{-2} Torr in an amorphous state. They were subsequently annealed at about 700 °C in 1 atm of air or oxygen to form $PdCoO_2$.[7] By PLD, $PdCoO_2$ has been formed directly during growth at pressures ranging from 10^{-1} to 2 Torr.[8,9] In the case of MBE, pressures of 4×10^{-6} Torr have been used.[10] The use of low pressures in MBE arises from the necessity of maintaining a mean-free-path that exceeds the distance from the sources to the substrate (typically ~20 cm) in order to preserve the molecular beams.[14]

When growing materials that are difficult to oxidize by MBE, a common approach to achieving oxidation at pressures within the MBE regime is to use activated oxidants, such as the reactive species emitted from an oxygen plasma source or concentrated ozone.[14] Brahlek *et al.*[10] used an atomic oxygen plasma in their recent MBE work. They found that they could oxidize the elemental constituents to form $PdCoO_2$ at substrate temperatures up to 300 °C, but that at higher growth temperatures, the $PdCoO_2$ spontaneously decomposed.[10] To improve the structural perfection and electrical transport properties of their films, Brahlek *et al.*[10] performed an *ex situ* anneal on their films. The best electrical properties were achieved following a 10 h anneal in 1 atm of oxygen at 800 °C. Although this anneal drastically improved the electrical transport, it also caused the film surface to roughen.[10]

In this study, we apply ozone-assisted MBE to the growth of $PdCoO_2$. Ozone is an excellent oxidant for use in MBE because it can be distilled and delivered with high purity to the substrate (~80% ozone with the remainder being oxygen).[15] In this concentrated ozone ambient, we find that $PdCoO_2$ films can be grown by MBE at substrate temperatures up to nearly 500 °C. At these significantly higher temperatures, the surface mobility of the adatoms is dramatically increased, leading to films with improved smoothness and structural perfection. Importantly, the films do not need to be annealed *ex situ* after growth. Our work thus opens the door to the growth of heterostructures and superlattices containing $PdCoO_2$ with an atomic-layer control as well as the possibility of achieving layers of sufficient quality that they can be characterized using in-vacuum techniques such as ARPES.[16]

The $PdCoO_2$ thin films are synthesized on *c*-plane sapphire at 480 °C (measured by a thermocouple close to, but not in direct contact with the substrate) under a chamber background pressure of 10^{-5} Torr of distilled ozone (~80% O_3 + 20% O_2) in a Veeco Gen10 MBE system. Palladium (99.999% purity) and cobalt (99.995% purity) are evaporated from Langmuir cells (free evaporation from crucibles with large orifices). The palladium and cobalt shutters are opened and closed sequentially under a continuous supply of ozone to supply monolayer doses of palladium and cobalt following the sequence of atomic layers along the *c*-axis of the crystal structure of $PdCoO_2$. Prior to the growth, the *c*-plane sapphire substrates (CrysTec GmbH) are annealed at 1050 °C under 1 atm of air for 6 h to obtain a step-and-terrace morphology. The planes of the substrates are all oriented within 0.2° of (0001). A summary of the samples studied, including thicknesses and electrical characteristics, is provided in Table I.

In situ reflection high-energy electron diffraction (RHEED) is employed to monitor the evolution of surface structures and reconstructions during growth. Figures 1(a) and 1(b) show the RHEED patterns of a bare *c*-plane sapphire substrate viewed along high symmetry directions where sharp diffraction streaks and Kikuchi lines are visible. Upon deposition of the first cobalt oxide monolayer followed by a palladium monolayer, the diffraction patterns change to those shown in Figs. 1(c) and 1(d). With the deposition of another cobalt oxide monolayer to complete the dumbbell O-Pd-O linear coordination along the *c*-axis (the direction of growth) of the bulk $PdCoO_2$ crystal structure, the diffraction patterns change again as shown in Figs. 1(e) and 1(f). Figures 1(g) and 1(h) show the RHEED patterns at the end of the growth of sample A, a 10.2 nm thick film. The latter RHEED patterns correspond to those of $PdCoO_2$ without any surface reconstruction, in contrast to the surface reconstructions present in Figs. 1(e) and 1(f) for the ultrathin CoO_2-Pd-CoO_2 film. Following two repeated cycles of supplying a monolayer of cobalt followed by a monolayer of palladium to the growing surface (under a continuous flux of ozone), the diffraction streaks are relatively sharp (and not spotty) indicating that our films are relatively smooth and epitaxial. In addition, we also observe splitting of the diffraction streaks into doublets which we do not yet fully understand, but attribute to the presence of in-plane rotational twins that are described below.

The morphology of the film surface is also characterized *ex situ* by atomic force microscopy (AFM) carried out using an Asylum Cypher ES Environmental AFM. Figure S1(a) in the supplementary material shows the step-and-terrace morphology of an annealed sapphire substrate with a root-mean-square (rms)

TABLE I. Summary of the samples studied in this letter and their features, including thickness, electrical characteristics, and the characterization techniques performed on them.

Sample	Thickness (nm)	$\rho_{ab(300\ K)}$ ($\mu\Omega$ cm)	RRR	Characterization
A	10.2 ± 0.2	9.3	2.2	XRD, *R* vs *T*, RHEED
B	8.0 ± 0.1	11	1.8	XRD, *R* vs *T*, AFM, STEM, RBS
C	5.4 ± 0.1	16	1.6	XRD, *R* vs *T*
D	4.1 ± 0.2	18	1.4	XRD, *R* vs *T*
E	3.2 ± 0.1	38	1.2	XRD, *R* vs *T*
F	2.0 ± 0.1	66	1.1	XRD, *R* vs *T*
G	1.6 ± 0.1	220	Insulating	XRD, *R* vs *T*, AFM

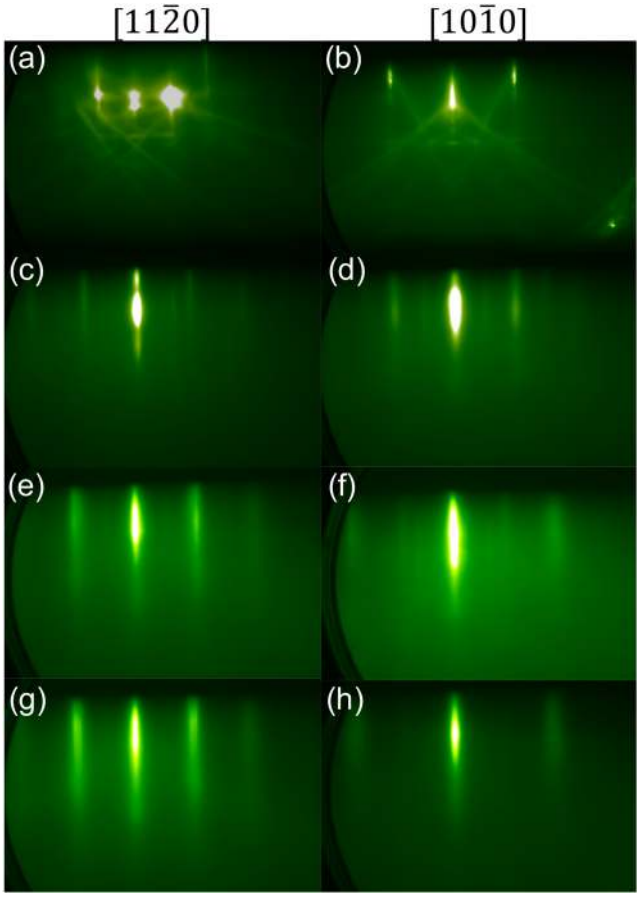

FIG. 1. RHEED patterns during the growth of sample A, a 10.2 nm thick $PdCoO_2$ film, along the azimuths indicated: (a) and (b) bare *c*-plane sapphire substrate, (c) and (d) after the deposition of the first CoO_2 and palladium monolayers (one of each), (e) and (f) after the deposition of CoO_2-Pd-CoO_2 monolayers to complete the O-Pd-O linear coordination, and (g) and (h) at the end of the growth.

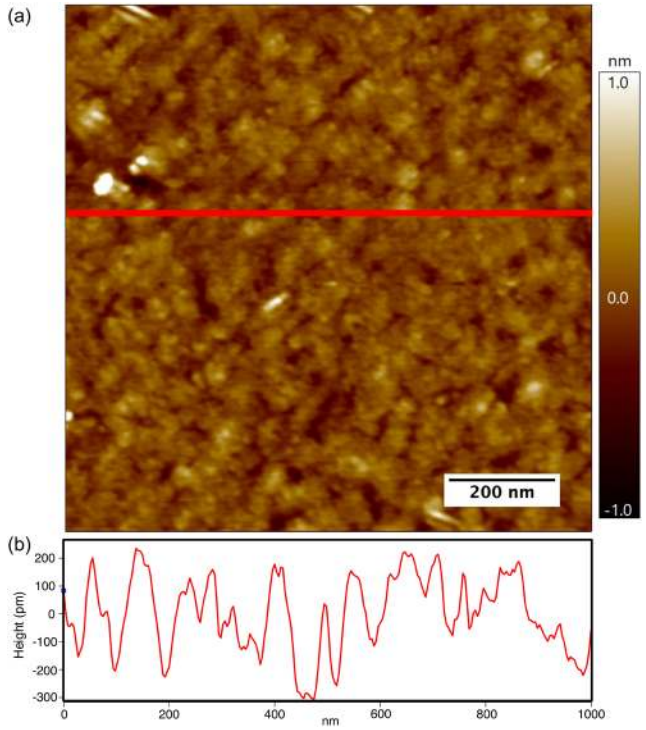

FIG. 2. AFM image of (a) sample B, an 8.0 nm thick $PdCoO_2$ film with a smooth surface morphology and a rms roughness of ~0.13 nm. (b) The height along a line profile corresponding to the red line drawn in (a).

roughness of 0.08 nm. After the deposition of the first three monolayers, deposited in the sequence cobalt, palladium, and cobalt in a continuous flux of ozone, the $PdCoO_2$ film has fully covered the substrate (the initial nuclei are fully coalesced), while the substrate steps are still apparent underneath, as shown in Fig. S1(b). At the end of the growth of sample B, the surface remains smooth with an rms roughness of 0.13 nm, as shown in Fig. S1(c) and in the magnified image in Fig. 2. Our films are the smoothest among $PdCoO_2$ thin films reported in the literature,[8,9] which will facilitate the controlled integration of this delafossite material with other materials as well as venturing into the atomic layer engineering of delafossites, which is now commonplace for perovskite oxides.

X-ray diffraction (XRD) measurements were carried out using Panalytical Empyrean and Panalytical X'Pert Pro diffractometers with Cu-$K_{\alpha 1}$ radiation. In the coupled θ-2θ scans in Fig. 3(a), only 000ℓ reflections corresponding to the bulk crystal structure of $PdCoO_2$ together with substrate reflections were observed, indicating that our films are *c*-axis oriented, epitaxial, and phase pure. Moreover, Laue oscillations around the film reflections are clearly visible, indicating that the films have a well-defined thickness, i.e., not only a smooth surface but also a smooth film-substrate interface. This is corroborated by the scanning transmission electron microscopy (STEM) image shown later in this letter. To study the structural perfection, we performed symmetric rocking curve measurements of the 0006 film and substrate reflections of sample B, using a triple-axis geometry. As shown in Fig. 3(b), the full width at half-maximum (FWHM) of the rocking curves in ω of the film and substrate reflections are comparable: both are 9 arc sec. This is the instrumental resolution of our diffractometer. Such a narrow rocking curve indicates the high degree of structural perfection in terms of a low out-of-plane mosaicity. In contrast to the narrow rocking curve in ω, the FWHM of the asymmetric ϕ scan shown in Fig. 3(d) is much larger for the film than that of the substrate (4800 arc sec and 470 arc sec, respectively). This indicates that the mosaic spread is highly anisotropic: there is far greater in-plane mosaic spread (twist) between $PdCoO_2$ subgrains than out-of-plane mosaic spread (tilt). Such asymmetry is observed in other heteroepitaxial systems such as GaN on (0001) Al_2O_3 and $SrTiO_3$ on (100) Si.[17,18] Both systems exhibit narrow out-of-plane ω-scan rocking curve widths and broader asymmetric ϕ-scan widths.

As illustrated in Fig. 3(c), by overlaying the in-plane crystal structures of *c*-axis oriented $PdCoO_2$ and Al_2O_3, we find a lattice

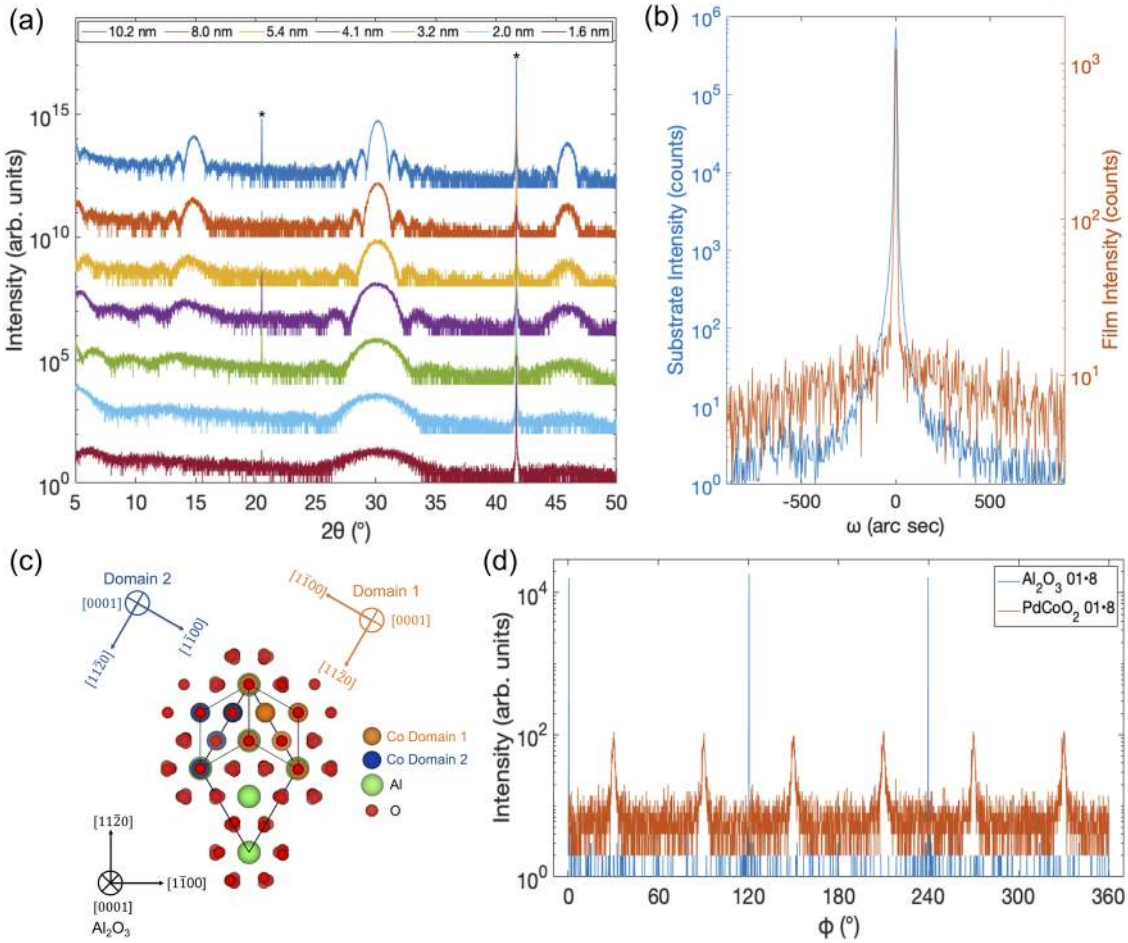

FIG. 3. X-ray diffraction (a) θ-2θ scans of samples A-G showing only 000ℓ reflections of $PdCoO_2$ and Laue oscillations indicating an abrupt and smooth film-substrate interface. Asterisks (*) denote substrate reflections. The scans are vertically offset from each other for clarity. (b) Overlaid rocking curves in ω of the 0006 film and substrate reflections of sample B; the comparable widths (9 arc sec for both the substrate and film) indicate low out-of-plane mosaicity. (c) In-plane epitaxial relationship between (0001) $PdCoO_2$ and (0001) Al_2O_3 showing the two $PdCoO_2$ domains with equivalent lattice mismatch with respect to Al_2O_3 and (d) off-axis ϕ scan of $01 \cdot 8$ reflections of $PdCoO_2$ and Al_2O_3 of sample A showing three poles for the substrate, but six poles for the film due to 180° in-plane rotation twinning.

mismatch of −2.9% under a 30° in-plane rotation,

$$\epsilon = \frac{a_{Al_2O_3} - \sqrt{3}a_{PdCoO_2}}{\sqrt{3}a_{PdCoO_2}} = \frac{4.76\ \text{Å} - 4.902\ \text{Å}}{4.902\ \text{Å}} = -2.9\%.$$

One implication that arises from this epitaxial orientation relationship is that there are two equivalent ways to lay the film crystal structure with respect to the substrate that are 180° rotated from each other. If this orientation relationship were true, we would expect rotational twinning in our films. We plot stereographic projections of the asymmetric $01 \cdot 8$ peaks of Al_2O_3 and $PdCoO_2$ in Fig. S2 where one only expects to see three equivalent poles for both the substrate and the film if both are untwinned single crystals. We performed an off-axis ϕ scan around the film and substrate $01 \cdot 8$ reflections of sample A. In addition to the three substrate peaks, six film peaks are present, as shown in Fig. 3(d). The film peaks are interpreted as two sets of peaks corresponding to domains that are 30° rotated from the substrate and 180° rotated from each other, which validates the orientation relationship proposed. The six peaks are all the same height, indicating equal populations of the two twin variants. These 180° in-plane rotation twins are consistent with prior studies of epitaxial $PdCoO_2$ grown on (0001) Al_2O_3 substrates.[8,10] The presence of these twin boundaries is likely detrimental to the electrical characteristics of our films, as discussed below.

High-angle annular dark field scanning transmission electron microscopy (HAADF-STEM) was performed on sample B using an aberration-corrected FEI Themis Titan microscope operating at 300 kV. Sample preparation was carried out by a focused ion beam (FIB) lift-out method using a Thermo Fisher Helios G4 UX FIB. From the cross-sectional HAADF-STEM images in Fig. S3 (low magnification) and Fig. 4(a) (high magnification), we observe an abrupt and smooth interface between the substrate and film,

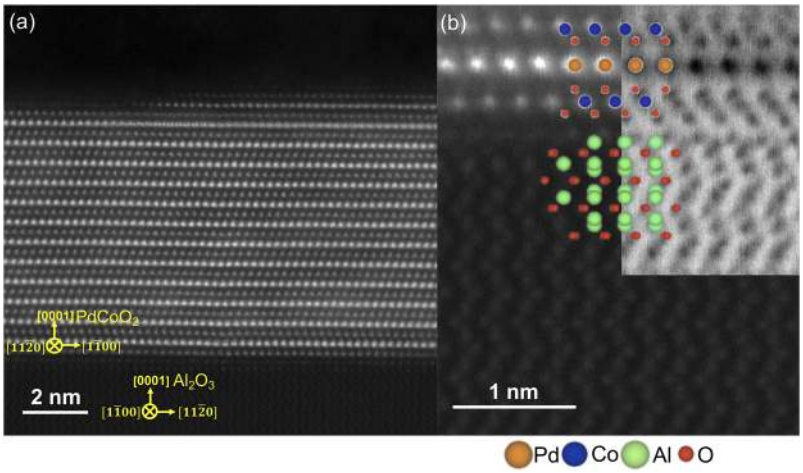

FIG. 4. (a) Cross-sectional HAADF-STEM image of sample B showing an abrupt interface between the Al_2O_3 substrate and the $PdCoO_2$ film. (b) Enlarged HAADF-STEM image with a simultaneously acquired ABF-STEM image in the inset near the substrate-interface region. The STEM images are overlaid by schematics of crystal structures of Al_2O_3 and $PdCoO_2$ showing the epitaxial relationship between the substrate and film with a 30° in-plane rotation. Note that the growth initiates with the CoO_2 layer on the (0001) Al_2O_3 surface.

consistent with the observation of the Laue oscillations mentioned earlier. Overlaid on the enlarged HAADF-STEM image near the film-substrate interface in Fig. 4(b) are an annular bright field (ABF-STEM) image and the schematics of the crystal structures of $PdCoO_2$ and Al_2O_3. We observe that the film structure is 30° rotated from the substrate, which is consistent with the XRD ϕ scans and prior reports.[8,10] From the XRD and STEM results, the epitaxial orientation relationship between the substrate and the film is determined to be (0001) $PdCoO_2$ || (0001) Al_2O_3 with [11$\bar{2}$0] $PdCoO_2$ || [1$\bar{1}$00] Al_2O_3 as well as a second in-plane twin variant with [11$\bar{2}$0] $PdCoO_2$ || [$\bar{1}$100] Al_2O_3. Owing to the atomic number contrast in the HAADF imaging mode, when combined with the ABF image, the brighter (dimmer) dots in the image and the orange (blue) spheres in the crystal structures are assigned to be palladium (and cobalt) atoms in Fig. 4(b), respectively. We observe that the first monolayer in contact with the sapphire substrate is indeed a CoO_2 layer followed by a palladium plane, which corresponds to the deposition sequence mentioned earlier. Note that the first monolayers in the PLD and *ex situ* annealed MBE films are also CoO_2 layers, suggesting the commonality of this feature in the heteroepitaxial $PdCoO_2/Al_2O_3$ system.[8,10] During growth we observe that if we deposit the palladium monolayer first or if we do not deposit a full cobalt monolayer, the resulting film is semicrystalline with weak diffracted features and a relatively intense diffuse background in RHEED, as shown in Fig. S4. This RHEED pattern does not improve with *in situ* annealing at temperatures up to 900 °C. This suggests that the palladium terminated surface of $PdCoO_2$ does not provide the low-energy interface in contact with *c*-plane sapphire; rather the CoO_2-terminated surface is the more stable interface with (0001)-oriented sapphire.

Rutherford backscattering spectrometry (RBS) using 1.4 MeV He^{4+} ions was used to assess the stoichiometry of the films. The results were analyzed using the software program RUMP.[19] The RBS spectrum of sample B is shown in Fig. S5. The Pd:Co ratio of this film is 1:1.05. Considering the accuracy of the RBS measurement for these films (±2%) and that the growth was both initiated and completed with a CoO_2 monolayer, we conclude that the film is stoichiometric to within the error bars of the RBS measurement.

We are particularly interested in exploring the transport in this two-dimensional electron system, $PdCoO_2$, at the ultrathin limit, a regime that is inaccessible using bulk crystals. We measured the transport properties of the MBE-grown films using a 4-point van der Pauw geometry[20] in a quantum design physical property measurement system (PPMS). Figure 5(a) shows the temperature dependence of the in-plane resistivity as a function of film thickness. The films are metallic down to ~2 nm and only becomes insulating at ~1.6 nm. This latter thickness contains fewer than 3 palladium planes along the *c*-axis of the film.

The residual resistivity ratio (RRR = $\rho_{300\ K}/\rho_{4\ K}$) is a sensitive probe to structural disorder as low temperature resistivity arises primarily from defects. As shown in Fig. 5(c), the RRRs of our films scale almost linearly with thickness, indicating that surface scattering has a large contribution to electrical resistance. For thin films, such boundaries include film-substrate interfaces and twin boundaries. The RRR of 2.2 of our thickest film (~10.2 nm) is comparable to the values of PLD-grown films at similar thicknesses,[8,9] but drastically inferior to the values of 16 and 347 for *ex situ* annealed MBE-grown films (180 nm thick) and single crystals, respectively.[10,21]

Note that the step height of our annealed sapphire substrate is ~0.26 nm, which corresponds to the Al-Al distance along the *c*-axis of sapphire, while the Co-Pd distance along the [0001] direction in $PdCoO_2$ is ~0.30 nm. This mismatch in the *c*-axis lengths could lead to the formation of out-of-phase boundaries[22] when palladium planes that nucleate on different steps of the sapphire substrate coalesce. The resulting discontinuities in palladium planes could disrupt the conduction pathways and deteriorate the electrical properties, which has been observed for other two dimensional metallic thin films.[23] The room temperature in-plane resistivity of our thickest film (~10.2 nm) is ~9.3 $\mu\Omega$ cm, which is several times larger than the single crystal value of 2.6 $\mu\Omega$ cm.[12] The room-temperature resistivity of our films increases quickly, however, with decreasing thickness reaching 220 $\mu\Omega$ cm at ~1.6 nm, as shown in Fig. 5(b). The increase in resistivity could also be attributed to a reduction in conduction pathways due to out-of-phase boundaries.

Besides out-of-phase boundaries and twin boundaries, the comparatively poorer electrical characteristics of our films could

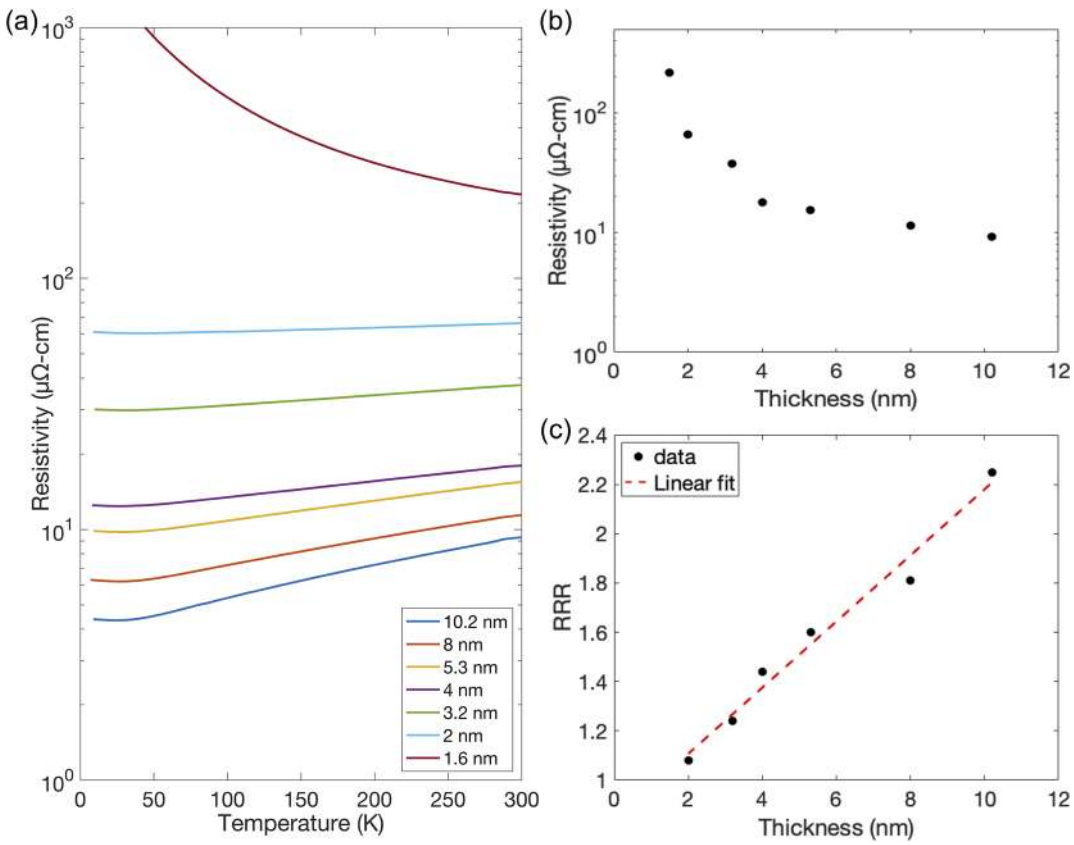

FIG. 5. Electrical transport measurements of $PdCoO_2$ films (samples A-G). (a) Temperature dependence of the in-plane resistivity showing the preservation of metallicity down to ~2 nm, which contains fewer than 4 palladium planes along the out-of-plane direction of the film. (b) Thickness dependence of the room-temperature in-plane resistivity showing an increase in resistivity at smaller thickness. (c) Thickness dependence of the residual resistivity ratio (RRR). RRR is seen to scale linearly with thickness, consistent with surface scattering.

arise because of additional crystallographic defects such as point defects associated with slight nonstoichiometry and dislocations due to the large lattice mismatch with the sapphire substrate. The higher defect densities of our films compared to the *ex situ* annealed MBE films could be attributed to the lower deposition temperature of 480 °C in our case vs the annealing temperature of 800 °C used in the latter work.[10] Higher annealing or growth temperature may aid the removal of defects to help improve the electrical properties. On the other hand, PdO becomes volatile at higher temperatures and we observe the formation of Co_3O_4 at growth temperatures higher than 500 °C. Indeed, the removal of crystallographic defects without losing PdO in single-step, *in situ* synthesis remains an open challenge. The other major contributors to low temperature resistivity, as mentioned earlier, are the twin boundaries.

In summary, we have grown *c*-axis oriented $PdCoO_2$ on *c*-plane sapphire using *in situ* MBE with distilled ozone as an oxidant. Our films are smooth and phase pure with a high degree of structural perfection and electrical characteristics similar to other *in situ* grown $PdCoO_2$ thin films in the literature. Using an ozone-assisted MBE approach, we have grown $PdCoO_2$ films exhibiting metallic conductivity as thin as in previous PLD work.[8] It is metallic at a film thickness of ~2.0 nm with fewer than 4 palladium monolayers along the out-of-plane direction. This ozone-assisted *in situ* MBE process provides the beginning of a pathway to atomically engineer delafossites for fundamental science purposes and to make and evaluate proof-of-principle device heterostructures.

See the supplementary material for additional characterization of the $PdCoO_2$ films by AFM, XRD, HAADF-STEM, RHEED, and RBS.

This work was primarily supported by the U.S. Department of Energy, Office of Basic Sciences, Division of Materials Sciences and Engineering, under Award No. DE-SC0002334. Materials synthesis was performed in a facility supported by the National Science Foundation [Platform for the Accelerated Realization, Analysis, and Discovery of Interface Materials (PARADIM)] under Cooperative Agreement No. DMR-1539918. This work made use of a Helios FIB supported by NSF (DMR-1539918) and the Cornell Center for Materials Research (CCMR) Shared Facilities, which are supported through the NSF MRSEC Program (Grant No. DMR-1719875). We would like to thank Malcolm Thomas, John

Grazul, and Mariena Silvestry Ramos for assistance in the Electron Microscopy CCMR facilities. The FEI Titan Themis 300 was acquired through Grant No. NSF-MRI-1429155, with additional support from Cornell University, the Weill Institute, and the Kavli Institute at Cornell. This work also made use of the CESI Shared Facilities partly sponsored by the NSF (Grant No. DMR-1338010) and the Kavli Institute at Cornell. Substrate preparation was performed in part at the Cornell NanoScale Facility, a member of the National Nanotechnology Coordinated Infrastructure (NNCI), which is supported by the NSF (Grant No. ECCS-1542081).

REFERENCES

[1] A. P. Mackenzie, Rep. Prog. Phys. **80**, 032501 (2017).
[2] V. Sunko, H. Rosner, P. Kushwaha, S. Khim, F. Mazzola, L. Bawden, O. J. Clark, J. M. Riley, D. Kasinathan, M. W. Haverkort, T. K. Kim, M. Hoesch, J. Fujii, I. Vobornik, A. P. Mackenzie, and P. D. C. King, Nature **549**, 492 (2017).
[3] S. Manipatruni, D. E. Nikonov, and I. A. Young, Nat. Phys. **14**, 338 (2018).
[4] C. T. Prewitt, R. D. Shannon, and D. B. Rogers, Inorg. Chem. **10**, 719 (1971).
[5] H. Takatsu, S. Yonezawa, S. Mouri, S. Nakatsuji, K. Tanaka, and Y. Maeno, J. Phys. Soc. Jpn. **76**, 104701 (2007).
[6] P. Kushwaha, V. Sunko, P. J. W. Moll, L. Bawden, J. M. Riley, N. Nandi, H. Rosner, M. P. Schmidt, F. Arnold, E. Hassinger, T. K. Kim, M. Hoesch, A. P. Mackenzie, and P. D. C. King, Sci. Adv. **1**, e1500692 (2015).
[7] P. F. Carcia, J. Electrochem. Soc. **127**, 1974 (1980).
[8] T. Harada, K. Fujiwara, and A. Tsukazaki, APL Mater. **6**, 046107 (2018).
[9] P. Yordanov, W. Sigle, P. Kaya, M. E. Gruner, R. Pentcheva, B. Keimer, and H.-U. Habermeier, Phys. Rev. Mater. **3**, 085403 (2019).
[10] M. Brahlek, G. Rimal, J. M. Ok, D. Mukherjee, A. R. Mazza, Q. Lu, H. Y. Lee, T. Z. Ward, R. Unocic, G. Eres, and S. Oh, Phys. Rev. Mater. **3**, 093401 (2019).
[11] T. Harada, S. Ito, and A. Tsukazaki, Sci. Adv. **5**, eaax5733 (2019).
[12] T. Harada, K. Sugawara, K. Fujiwara, S. Ito, T. Nojima, T. Takahashi, T. Sato, and A. Tsukazaki, e-print arXiv:1908.08173 (unpublished).
[13] D. B. Rogers and R. D. Shannon, "Electrically conductive oxides containing palladium and their preparation," U.S. patent 3,514,414 (3 March 1970).
[14] D. G. Schlom and J. S. Harris, Jr., "MBE growth of high T_c superconductors," in *Molecular Beam Epitaxy: Applications to Key Materials*, edited by R. F. C. Farrow (Noyes, Park Ridge, 1995), pp. 505–622.
[15] C. D. Theis and D. G. Schlom, "The reactivity of ozone incident onto the surface of perovskite thin films grown by MBE," in *High Temperature Materials Chemistry IX*, edited by K. E. Spear (Electrochemical Society, Pennington, 1997), Vol. 97-39, pp. 610–616.
[16] E. J. Monkman, C. Adamo, J. A. Mundy, D. E. Shai, J. W. Harter, D. Shen, B. Burganov, D. A. Muller, D. G. Schlom, and K. M. Shen, Nat. Mater. **11**, 855 (2012).
[17] B. Heying, X. H. Wu, S. Keller, Y. Li, D. Kapolnek, B. P. Keller, S. P. DenBaars, and J. S. Speck, Appl. Phys. Lett. **68**, 643 (1996).
[18] Z. Wang, B. H. Goodge, D. J. Baek, M. J. Zachman, X. Huang, X. Bai, C. M. Brooks, H. Paik, A. B. Mei, J. D. Brock, J.-P. Maria, L. F. Kourkoutis, and D. G. Schlom, Phys. Rev. Mater. **3**, 073403 (2019).
[19] See http://www.genplot.com/RUMP/index.htm for information on the RUMP software used to analyze RBS spectrum.
[20] L. J. van der Pauw, Philips Res. Rep. **20**, 220 (1958).
[21] C. W. Hicks, A. S. Gibbs, A. P. Mackenzie, H. Takatsu, Y. Maeno, and E. A. Yelland, Phys. Rev. Lett. **109**, 116401 (2012).
[22] M. A. Zurbuchen, W. Tian, X. Q. Pan, D. Fong, S. K. Streiffer, M. E. Hawley, J. Lettieri, Y. Jia, G. Asayama, S. J. Fulk, D. J. Comstock, S. Knapp, A. H. Carim, and D. G. Schlom, J. Mater. Res. **22**, 1439 (2007).
[23] H. P. Nair, J. P. Ruf, N. J. Schreiber, L. Miao, M. L. Grandon, D. J. Baek, B. H. Goodge, J. P. C. Ruff, L. F. Kourkoutis, K. M. Shen, and D. G. Schlom, APL Mater. **6**, 101108 (2018).